INTERNATIONAL JOURNAL FOR NUMERICAL METHODS IN FLUIDS, VOL. 26, 345–364 (1998)

COMPUTATION OF PARTICLE DISPERSION IN TURBULENT LIQUID FLOWS USING AN EFFICIENT LAGRANGIAN TRAJECTORY MODEL

X.-Q. CHEN* AND J.C.F. PEREIRA

Section of Applied Thermodynamics, Mechanical Engineering Department, Instituto Superior Técnico/Technical University of Lisbon, 1096 Lisbon Codex, Portugal

SUMMARY

The dispersion of solid particles in a turbulent liquid flow impinging on a centrebody through an axisymmetric sudden expansion was investigated numerically using a Eulerian–Lagrangian model. Detailed experimental measurements at the inlet were used to specify the inlet conditions for two-phase flow computations. The anisotropy of liquid turbulence was accounted for using a second-moment Reynold stress transport model. A recently developed stochastic–probabilistic model was used to enhance the computational efficiency of Lagrangian trajectory computations. Numerical results of the stochastic–probabilistic model using 650 particle trajectories were compared with those of the conventional stochastic discrete-delta-function model using 18 000 particle trajectories. In addition, results of the two models were compared with experimental measurements. © 1998 John Wiley & Sons, Ltd.

Int. J. Numer. Meth. Fluids **26**: 345–364 (1998)

KEY WORDS: liquid–particle flow; computational efficiency; Eulerian–Lagrangian model

1. INTRODUCTION

Dispersed liquid–solid flows find wide applications in a variety of industrial processes, e.g. hydrocyclones and hydraulic conveying, and in hydroelectric engineering, where water turbines are often operated in silt-laden rivers. Therefore it is of great importance to study such a category of two-phase flows.

Dispersed two-phase flows are characterized by the presence of a continuous phase and a particulate phase. As one of the widely adopted numerical approaches for handling particulate two-phase flows, the Eulerian–Lagrangian model treats the continuous phase using a Eulerian formulation and the dispersed phase using a Lagrangian formulation. The dispersion of discrete particles due to the continuous phase turbulence is accounted for by a stochastic procedure. Numerical investigations of two-phase flows can be found in References [1–8], among others. A recent complete review of numerical models for two-phase turbulent flows can be found in Reference [9].

For the computation of laminar two-phase flows, no Lagrangian stochastic model is required [10]. The recent computation of an unsteady water droplet spray [11] also neglected

* Correspondence to: Section of Applied Thermodynamics, Mechanical Engineering Department, Instituto Superior Técnico/Technical University of Lisbon, 1096 Lisbon Codex, Portugal. E-mail: dsc34-18@beta.ist.utl.pt

Contract grant sponsor: JNICT (Portugal)

CCC 0271–2091/98/030345–20$17.50 *Received January 1997*

the effect of fluid turbulence on droplet dispersion. However, a stochastic Lagrangian trajectory model has to be used when computing turbulent two-phase flows using a Eulerian–Lagrangian hybrid model; otherwise, particle dispersion will be seriously underpredicted. It is widely recognized, however, that the Lagrangian stochastic model often requires computing thousands of individual particle trajectories to attain a stochastically significant solution. Mostafa *et al.* [12] reported that 100 000 particle trajectories were necessary for computing the monodispersed particle laden jet. Adeniji-Fashola and Chen [13] achieved the smoothest profiles of predictions using a total of 9000 computational particle trajectories for a confined particle-laden jet. Chang and Wu [6] found that a large number (20 000) of droplet trajectories were required to reach an invariant solution for the polydispersed hollow cone spray. Chen and Pereira [14] performed a study of the sensitivity of droplet properties to various parameters, including the number of droplet trajectories, for the turbulent evaporating spray. It was found that 10 000 droplet trajectories were necessary to achieve an invariant solution for the turbulent, polydispersed, evaporating spray. Recently, Sato *et al.* [7] employed about 33 000 particle trajectories to compute a monosized particle-laden planar turbulent jet. Obviously, the more particle trajectories that are tracked, the more computer CPU time will be required for the Lagrangian solver; therefore it is probable that computations of three-dimensional dispersed turbulent two-phase flows will require hundred of thousands of particle trajectories.

Evidently, to compute dispersed turbulent two-phase flows, an approach is needed which is efficient in computation, accurate in prediction and simple in theoretical background. To this end, a new *stochastic–probabilistic efficiency-enhanced dispersion* (SPEED) model was developed by Chen and Pereira [15], seeking to track a relatively small number of particle trajectories but offering computational noise-free or noise-reduced solution. The SPEED model adopts the conventional stochastic discrete-delta-function (SDDF) model developed by Gosman and Ioannides [16], but it is distinguished from the SDDF model because an additional probabilistic model is developed to account for the probabilistic distribution of a physical particle in space. Such a stochastic–probabilistic algorithm is aimed at realizing the objective of achieving a stochastically significant solution by tracking a minimum number of particle trajectories. As a consequence, the computational efficiency of Lagrangian trajectory calculations can be greatly enhanced.

Another aspect related to the Eulerian–Lagrangian model is that the accuracy of its numerical predictions is often limited by the uncertainty of incomplete experimentally specified initial conditions; as a result, the specification of detailed inlet conditions for Lagrangian computations plays an important role in appropriately assessing Lagrangian stochastic models [17–19]. Evidently, the validation of two-phase flow models is unfavourably influenced by the uncertainty of assuming inlet conditions. Therefore the present two-phase flow predictions were carried out using available complete initial conditions from measurements.

The objective of this study is to investigate a dilute particle-laden turbulent liquid flow using the efficient SPEED model of Chen and Pereira [15]. This model includes both stochastic and probabilistic computations. The stochastic computation of particle trajectories, obtained with a conventional stochastic model, determines the motion of the locus of the trajectory centre, while the probabilistic computation of trajectory variances, obtained with an additional ordinary differential equation, determines the spatial distribution of physical particles. Well-specified experimental measurements [20] for a dispersed liquid–solid flow were used to provide complete initial conditions for two-phase flow computations; as a result, the uncertainty of inlet conditions on model validation was ruled out. The computational efficiency and accuracy of the SPEED model are assessed by making comparisons with the stochastic discrete-delta-function model and experimental measurements.

2. EULERIAN EQUATION FOR LIQUID PHASE

Most of the existing turbulence models for the continuous phase in two-phase flow predictions are based on the k–ε model [3,6]. However, this turbulence model cannot account for the anisotropy of turbulence, which is observed in the flow investigated here. Therefore the second-moment Reynolds stress closure model was used for the fluid phase to better account for the anisotropy of turbulence. The governing equations for mass, momentum and Reynolds stresses can be written tensorially as

$$\frac{\partial \rho U_j}{\partial x_j} = 0, \tag{1}$$

$$\frac{\partial \rho U_i U_j}{\partial x_j} = -\frac{\partial P}{\partial x_i} + \frac{\partial}{\partial x_j}\left(\mu \frac{\partial U_i}{\partial x_j} - \rho \overline{u_i u_j}\right) + S^{\mathrm{p}}_{U_i}, \tag{2}$$

$$\frac{\partial}{\partial x_k}(\rho U_k \overline{u_i u_j}) = \frac{\partial}{\partial x_k}\left[\left(\mu \delta_{mk} + \rho C_{\mathrm{s}} \frac{k}{\varepsilon} \overline{u_k u_m}\right) \frac{\partial \overline{u_i u_j}}{\partial x_m}\right] + P_{ij} - \frac{2}{3}\rho \varepsilon \delta_{ij} + \phi_{ij} + S^{\mathrm{p}}_{\overline{u_i u_j}}, \tag{3}$$

where P_{ij} and ϕ_{ij} denote the generation and the pressure–strain correlation respectively. The generation term is defined as

$$P_{ij} = -\rho \overline{u_j u_k} \frac{\partial U_i}{\partial x_k} - \rho \overline{u_i u_k} \frac{\partial U_j}{\partial x_k}. \tag{4}$$

The pressure–strain correlation term ϕ_{ij} consists of a slow part $\phi_{ij,1}$ and a fast part $\phi_{ij,2}$, as well as their corresponding near-wall modifications $\phi^{\mathrm{w}}_{ij,1}$ and $\phi^{\mathrm{w}}_{ij,2}$, i.e.

$$\phi_{ij} = \phi_{ij,1} + \phi_{ij,2} + \phi^{\mathrm{w}}_{ij,1} + \phi^{\mathrm{w}}_{ij,2}, \tag{5}$$

$$\phi_{ij,1} = -C_1 \rho \frac{\varepsilon}{k}\left(\overline{u_i u_k} - \frac{2}{3} k \delta_{ij}\right), \qquad \phi_{ij,2} = -C_2\left(P_{ij} - \frac{2}{3} G \delta_{ij}\right), \tag{6}$$

where the production $G = P_{kk}/2$. The near-wall isotropization of production is given by

$$\phi^{\mathrm{w}}_{ij,1} = C'_1 \rho \frac{\varepsilon}{k}\left(\overline{u_l u_m} n_l n_m \delta_{ij} - \frac{3}{2}\overline{u_l u_i} n_l n_j - \frac{3}{2}\overline{u_l u_j} n_l n_i\right) f_k, \tag{7}$$

$$\phi^{\mathrm{w}}_{ij,2} = C'_2\left(\phi_{lm,2} n_l n_m \delta_{ij} - \frac{3}{2}\phi_{il,2} n_l n_j - \frac{3}{2}\phi_{jl,2} n_l n_j\right) f_k, \tag{8}$$

where n_i stands for the unit vector of the i-component normal to the wall; the subscript k takes the same value as l but without summation. The two components of the function f_k are given by

$$f_x = 0.41 k^{1.5}/\varepsilon x_{\mathrm{w}}, \qquad f_y = 0.41 k^{1.5}/\varepsilon y_{\mathrm{w}}. \tag{9}$$

The source terms $S^{\mathrm{p}}_{U_i}$ and $S^{\mathrm{p}}_{\overline{u_i u_j}}$ arise from the liquid–particle interactions and are determined in Lagrangian trajectory computations. A description of the terms can be found elsewhere [3,14]. The equation for the dissipation rate of the turbulent kinetic energy is

$$\frac{\partial}{\partial x_j}(\rho U_j \varepsilon) = \frac{\partial}{\partial x_j}\left(\mu \frac{\partial \varepsilon}{\partial x_j} + C_\varepsilon \rho \frac{k}{\varepsilon} \overline{u_i u_j} \frac{\partial \varepsilon}{\partial x_i}\right) + \frac{\varepsilon}{k}(C_{\varepsilon 1} G - C_{\varepsilon 2} \rho \varepsilon) + C_{\varepsilon 3} \frac{\varepsilon}{k} S^{\mathrm{p}}_k, \tag{10}$$

where the turbulence modulation term is given by

$$S^{\mathrm{p}}_k = 0.5 S^{\mathrm{p}}_{\overline{u_j u_j}}. \tag{11}$$

The values of the model constants used in the foregoing equations are $(C_s, C_1, C_2, C_1', C_2', C_\varepsilon, C_{\varepsilon 1}, C_{\varepsilon 3}) = (0.22, 1.8, 0.6, 0.5, 0.3, 0.15, 1.45, 1.9, 1.1)$.

3. LAGRANGIAN EQUATIONS FOR PARTICLE PHASE

To account for the lift force induced by the fluid velocity gradient, the lift force is included in the equation of motion of a particle, together with the drag and gravity forces. In addition, the relatively lower ratio of the particle density to the water density requires including the added mass term. As a result, the equation of motion for each of the representative particle sizes can be written tensorially as

$$\frac{\mathrm{d}\tilde{U}_{\mathrm{p}i}}{\mathrm{d}t} = \frac{\tilde{U}_i - \tilde{U}_{\mathrm{p}i}}{\tau_{\mathrm{p}}} + \left(1 - \frac{\rho}{\rho_{\mathrm{p}}}\right) g_i + \frac{\rho}{2\rho_{\mathrm{p}}} \frac{\mathrm{d}}{\mathrm{d}t}(\tilde{U}_i - \tilde{U}_{\mathrm{p}i}) + \frac{3.0844}{\rho_{\mathrm{p}} D_{\mathrm{p}}} \sqrt{\left(\rho\mu \left|\frac{\partial \tilde{U}_j}{\partial x_m}\right|\right)} (\tilde{U}_j - \tilde{U}_{\mathrm{p}j})(1 - \delta_{mj})\delta_{mi}, \tag{12}$$

where $\tilde{U}_i$ is the fluid (liquid) instantaneous velocity. The relaxation time of a particle, τ_{p}, is defined as

$$\tau_{\mathrm{p}} = \rho_{\mathrm{p}} D_{\mathrm{p}}^2 / 18\mu f_{\mathrm{p}}, \tag{13}$$

where the drag correction coefficient f_{p} is determined by

$$f_{\mathrm{p}} = 1 + 0.15 Re_{\mathrm{p}}^{0.687} \quad (0 < Re_{\mathrm{p}} < 1000). \tag{14}$$

The relative Reynolds number in (14) is defined as

$$Re_{\mathrm{p}} = \rho V_{\mathrm{rel}} D_{\mathrm{p}} / \mu, \tag{15}$$

with V_{rel} being the relative velocity between the two phases. The particle trajectories are computed by

$$\frac{\mathrm{d}x_{\mathrm{p}i}}{\mathrm{d}t} = \tilde{U}_{\mathrm{p}i}. \tag{16}$$

Note that it is impossible to determine the fluid instantaneous velocity gradient $\partial \tilde{U}_j / \partial x_m$ in (12) at the particle position; therefore the mean fluid velocity gradient was used. Such a treatment is similar to the method of Sato *et al.* [7], who used the fluid instantaneous velocity at the particle position and the mean fluid velocity on the Eulerian grid near the particle to estimate the velocity gradient.

4. STOCHASTIC–PROBABILISTIC PARTICLE DISPERSION MODEL

The stochastic–probabilistic trajectory model consists of both stochastic and probabilistic computations. The stochastic computation basically follows the approach of Reference [16] by using the instantaneous continuous phase velocity to account for the effects of particle dispersion induced by continuous phase turbulence. However, the fluctuating velocity is randomly sampled from local turbulent normal stresses, instead of the local turbulent kinetic energy, in terms of particle–eddy encounters to account for the anisotropy of turbulence on particle dispersion, as discussed by Chen and Pereira [14]. Even though such a modification has

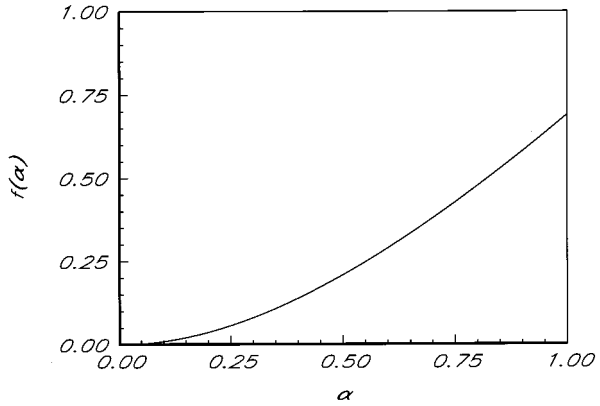

Figure 1. Variation of exponential function with integral time

accounted for the effects of the anisotropy of turbulence on particle dispersion, there still exists another deficiency that a 'too large' number of particle trajectories are necessarily tracked to achieve a stochastically significant or invariant solution, thus consuming a great amount of computer CPU time. This can be explained as follows. In the conventional Lagrangian stochastic model the particle trajectory computed with (16) represents a single point in space. In other words, the discrete-delta-function model is used for the distribution of a physical particle in space; therefore it requires tracking too many individual particle trajectories to achieve the stochastically significant solution.

To enhance the computational efficiency, the SPEED model is used, which performs a probabilistic computation, in addition to the stochastic computation, at each Lagrangian time step along a particle trajectory. The probabilistic computation is based on a computed trajectory variance and an assumed probability density function. The equation governing the particle trajectory variance can be derived from its definition [15]. The final equation can be written tensorially as

$$\frac{\mathrm{d}\sigma_{\mathrm{p}i}^2}{\mathrm{d}t} = 2\delta_{ij} \int_0^t \langle u_{\mathrm{p}j}(t) u_{\mathrm{p}j}(t_1) \rangle \, \mathrm{d}t_1, \tag{17}$$

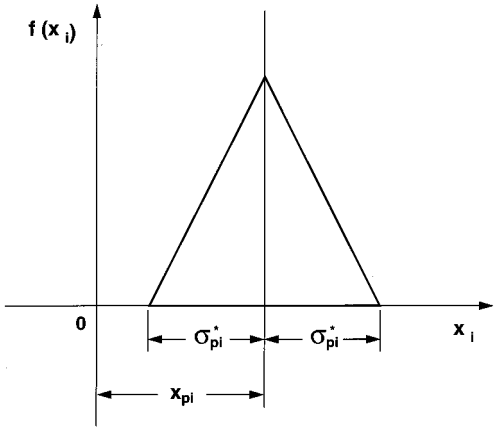

Figure 2. Isosceles triangle probability density function

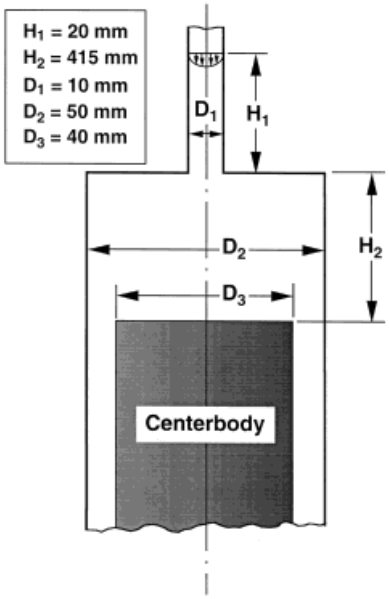

Figure 3. Configuration of axisymmetric sudden-expansion flow

where $\langle\ \rangle$ denotes the ensemble-averaging procedure and $\langle u_{pj}(t)u_{pj}(t_1)\rangle$ represents the correlation of particle velocity fluctuations between time intervals t and t_1. Evidently, no direct information is available for this particle velocity correlation along its trajectory. However, the use of a turbulence closure model (namely the Reynolds stress model) can provide us with the predicted Reynolds stresses of the continuous phase. Therefore an expression may be derived to relate the velocity fluctuations of the particle phase to those of the fluid phase, i.e.

$$\langle u_{pj}(t)u_{pj}(t_1)\rangle = \Omega_{pj}\langle u_j(t)u_j(t_1)\rangle \quad \text{(no summation)}, \tag{18}$$

where $\langle u_j(t)u_j(t_1)\rangle$ represents the correlation of the velocity fluctuations for fluid tracers and Ω_{pj} accounts for the slipping effects between the two phases and is necessarily determined. This problem is similar to the modelling of particle turbulent viscosity in the twin-fluid modelling of particle-laden turbulent flows [13,21]. Following Rizk and Elghobashi [21], this parameter can be estimated by

$$\Omega_{pi} = \sigma_p\left(1 + C_\beta \frac{V_{rel}^2}{\langle u_i^2\rangle}\right)^{-0.5}, \tag{19}$$

where $\langle u_i^2\rangle$ is the normal stress component at the particle position. The model constants C_β and σ_p are necessarily estimated. Of course, other expressions may also be possible, as long as they can adequately account for the two-phase slipping effects. To determine the fluid velocity correlation, a Lagrangian autocorrelation function $R_{Li}(\tau)$ is used,

$$R_{Li}(\tau) = \frac{\langle u_j(t)u_j(t+\tau)\rangle}{\langle u_j^2(t)\rangle}\,\delta_{ij}, \tag{20}$$

where $\tau = t_1 - t$. Following Berlemont *et al.* [3], the autocorrelation function can be estimated using a Frenkiel correlation function as

$$R_{\mathrm{L}i}(\tau) = \cos\left(\frac{\tau}{2T_{\mathrm{L}j}}\right)\exp\left(-\frac{\tau}{2T_{\mathrm{L}j}}\right)\delta_{ij}, \tag{21}$$

where the integral time scale for each component is determined by

$$T_{\mathrm{L}i} = 0.235\langle u_i^2\rangle/\varepsilon. \tag{22}$$

Introducing (21) into (17) and performing integration in part, Equation (17) can be rewritten as

$$\frac{\mathrm{d}\sigma_{\mathrm{p}i}^2}{\mathrm{d}t} = 2\Omega_{\mathrm{p}j}\delta_{ij}\langle u_j^2\rangle T_{\mathrm{L}j}\left\{1-\exp\left(-\frac{t}{2T_{\mathrm{L}j}}\right)\left[\cos\left(\frac{t}{2T_{\mathrm{L}j}}\right)-\sin\left(\frac{t}{2T_{\mathrm{L}j}}\right)\right]\right\}. \tag{23}$$

Under the assumption that a very small time step Δt is used, Equation (23) can be approximately integrated [22] as

$$\sigma_{\mathrm{p}i}^2(t+\Delta t) = \sigma_{\mathrm{p}i}^2(t) + 2\Omega_{\mathrm{p}j}\delta_{ij}\langle u_j^2\rangle T_{\mathrm{L}j}\left[\Delta t - 2T_{\mathrm{L}j}\exp\left(-\frac{\Delta t}{2T_{\mathrm{L}j}}\right)\sin\left(\frac{\Delta t}{2T_{\mathrm{L}j}}\right)\right]. \tag{24}$$

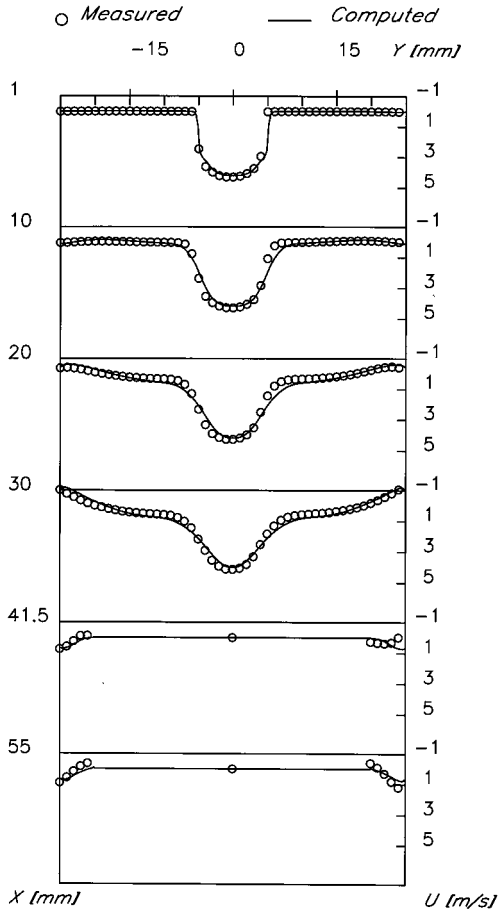

Figure 4. Measured and predicted liquid streamwise mean velocity

It can be proven that the right-hand side of (24) is always positive, as physically required. Shown in Figure 1 is the vibration of $f(\alpha) = 1 - \exp(-\alpha)\sin\alpha$ with α, where α is defined as $\Delta t/2T_{Lj}$. Note that the Lagrangian advance step for integration is chosen in such a way that it is always smaller than 20% of the integral time scale.

It should be stressed that the trajectory determined with (16) only represents the locus of the trajectory centre at each Lagrangian advance step for the SPEED model. Simultaneously, particle trajectory variances are determined from (17) to account for the dispersive effect induced by turbulence. Therefore, given a probability density function (PDF) $f(x, y)$, the distribution of a physical particle in Eulerian control volumes can be determined. It follows that the ensemble-averaged particle property can be obtained by

$$\phi(x, y) = \frac{\sum_{k=1}^{M} \dot{N}_k \, \Delta t_k \int_{x^1}^{x^u} \int_{y^1}^{y^u} \phi_k(x_p, y_p) f_k(x, y) \, dx \, dy}{\sum_{k=1}^{M} \dot{N}_k \, \Delta t_k \int_{x^1}^{x^u} \int_{y^1}^{y^u} f_k(x, y) \, dx \, dy}, \tag{25}$$

where the summation over k represents all the particle sizes crossing the Eulerian control volume in question, with M being the total number of particle trajectories. $\dot{N}_k$ in (25) denotes the particle number flow rate of the kth particle and the product of $\dot{N}_k$ and Δt_k stands for the total number of particles in the Eulerian control volume. The two-way coupling source is computed by

$$S_\phi^p(x, y) = \sum_{k=1}^{M} \dot{N}_k \, \Delta t_k \int_{x^1}^{x^u} \int_{y^1}^{y^u} S_{\phi_k}^p(x_p, y_p) f_k(x, y) \, dx \, dy, \tag{26}$$

where $S_{\phi_k}^p$ is determined in Lagrangian trajectory computations via two-way coupling expressions in terms of exchanges in momentum and energy. Note that (x_p, y_p) in (25) and (26) represents the current particle position and that a prescribed PDF is required to determine the particle probability distribution in these equations. The Gaussian PDF may be one of the adequate PDFs to represent a variety of flows. However, Litchford and Jeng [23] carried out a sensitivity study of the effects of PDF shapes on Lagrangian computations and found that a simplified isosceles triangle PDF may replace the Gaussian PDF, thus enhancing the code efficiency. Therefore the isosceles triangle PDF, as shown in Figure 2, is used for the present study. It should be pointed out that the SPEED model is different from the stochastic dispersion width transport model of Litchford and Jeng [24], in that the SPEED model determines the trajectory variance using the ordinary differential equation, i.e. (17), whereas the stochastic dispersion width transport model computes the dispersions width using the concept of particle–eddy encounters, which involves many repeated summing operations, as discussed by Chen and Pereira [25]. Consequently, the SPEED model offers higher computational efficiency than the stochastic dispersion width transport model.

Given the trajectory mean and variance, the isosceles triangle probability density function can be determined. However, particular attention should be paid to computing the radial component of the cumulative distribution function for axisymmetric flow configurations. The axisymmetric cumulative function at any radius r is defined as the volume swept out by the planar region of the PDF bounded between $-r$ and r as it is revolved 360° about the axis of symmetry [23]. Detailed discussion of this issue can be found in Reference [24]. The final cumulative distribution function for the radial component at any radial position r can be determined as follows.

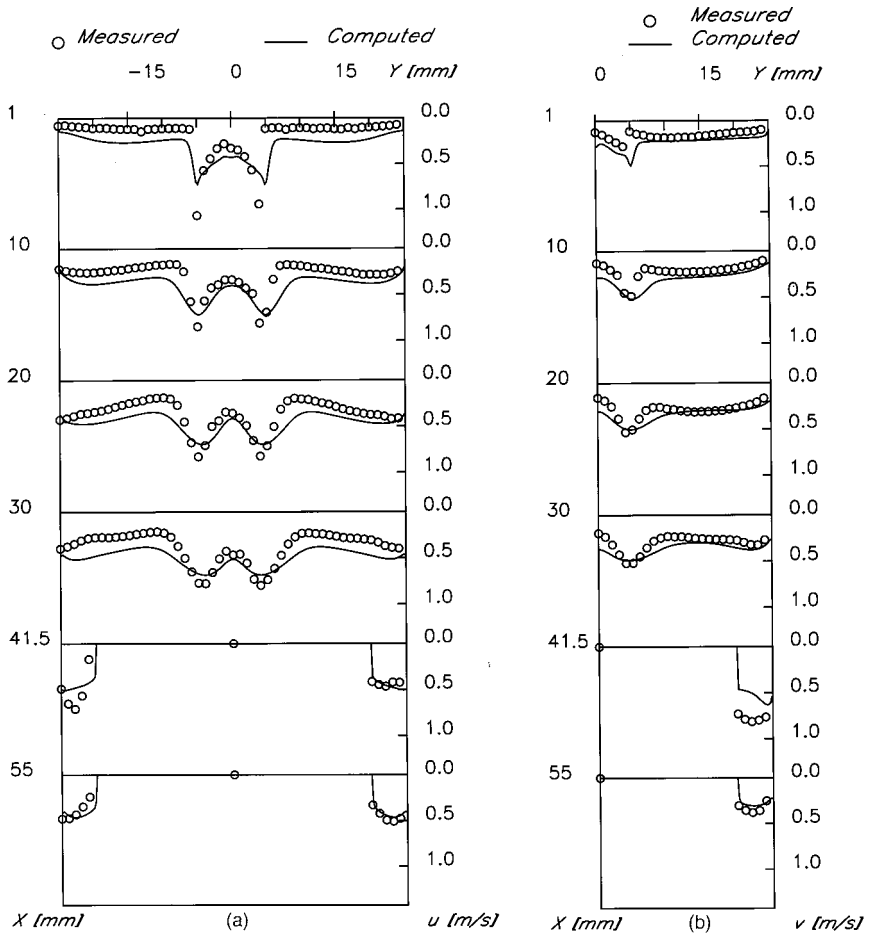

Figure 5. Measured and predicted liquid (a) streamwise and (b) radial RMS velocities

Case 1

$$P(r)=\begin{cases} P_{\mathrm{a}}(r), & 0<r<\sigma^{*}_{\mathrm{p}r}-r_{\mathrm{p}},\\ P_{\mathrm{b}}(r), & \sigma^{*}_{\mathrm{p}r}-r_{\mathrm{p}}<r<r_{\mathrm{p}},\\ P_{\mathrm{c}}(r), & \sigma^{*}_{\mathrm{p}r}-r_{\mathrm{p}}<r<\sigma^{*}_{\mathrm{p}r}+r_{\mathrm{p}},\\ 1, & r\geq\sigma^{*}_{\mathrm{p}r}+r_{\mathrm{p}}, \end{cases} \quad \text{for } \sigma^{*}_{\mathrm{p}r}/2<r_{\mathrm{p}}<\sigma^{*}_{\mathrm{p}r}. \tag{27}$$

Case 2

$$P(r)=\begin{cases} P_{\mathrm{a}}(r), & 0<r<r_{\mathrm{p}},\\ P_{\mathrm{b}}(r), & r_{\mathrm{p}}<r<\sigma^{*}_{\mathrm{p}r}-r_{\mathrm{p}},\\ P_{\mathrm{d}}(r), & \sigma^{*}_{\mathrm{p}r}-r_{\mathrm{p}}<r<\sigma^{*}_{\mathrm{p}r}+r_{\mathrm{p}},\\ 1, & r\geq\sigma^{*}_{\mathrm{p}r}+r_{\mathrm{p}}, \end{cases} \quad \text{for } \ 0<r_{\mathrm{p}}<\sigma^{*}_{\mathrm{p}r}/2. \tag{28}$$

Case 3

$$P(r)=\begin{cases}0, & 0<r<r_{\mathrm{p}}-\sigma^{*}_{\mathrm{p}r},\\ P_{\mathrm{c}}(r), & r_{\mathrm{p}}-\sigma^{*}_{\mathrm{p}r}<r<r_{\mathrm{p}},\\ P_{\mathrm{e}}(r), & r_{\mathrm{p}}<r<\sigma^{*}_{\mathrm{p}r}+r_{\mathrm{p}},\\ 1, & r\geq\sigma^{*}_{\mathrm{p}r}+r_{\mathrm{p}},\end{cases}\quad \text{for}\quad r_{\mathrm{p}}>\sigma^{*}_{\mathrm{p}r}. \tag{29}$$

Here the terms P_{a}, P_{b}, P_{c}, P_{d} and P_{e} are given by

$$P_{\mathrm{a}}(r)=\frac{6|\sigma^{*}_{\mathrm{p}r}-r_{\mathrm{p}}|r^{2}}{-2r_{\mathrm{p}}^{3}+(\sigma^{*}_{\mathrm{p}r}+r_{\mathrm{p}})^{3}+|\sigma^{*}_{\mathrm{p}r}-r_{\mathrm{p}}|^{3}},\qquad P_{\mathrm{b}}(r)=\frac{-4r^{3}+6\sigma^{*}_{\mathrm{p}r}r^{2}-2r_{\mathrm{p}}^{3}}{-2r_{\mathrm{p}}^{3}+(\sigma^{*}_{\mathrm{p}r}+r_{\mathrm{p}})^{3}+|\sigma^{*}_{\mathrm{p}r}-r_{\mathrm{p}}|^{3}},$$

$$P_{\mathrm{c}}(r)=\frac{2r^{3}+3|\sigma^{*}_{\mathrm{p}r}-r_{\mathrm{p}}|r^{2}+|\sigma^{*}_{\mathrm{p}r}-r_{\mathrm{p}}|^{3}}{-2r_{\mathrm{p}}^{3}+(\sigma^{*}_{\mathrm{p}r}+r_{\mathrm{p}})^{3}+|\sigma^{*}_{\mathrm{p}r}-r_{\mathrm{p}}|},$$

$$P_{\mathrm{d}}(r)=\frac{-2r^{3}+3(\sigma^{*}_{\mathrm{p}r}+r_{\mathrm{p}})r^{2}-2r_{\mathrm{p}}^{3}+|\sigma^{*}_{\mathrm{p}r}-r_{\mathrm{p}}|^{3}}{-2r_{\mathrm{p}}^{3}+(\sigma^{*}_{\mathrm{p}r}+r_{\mathrm{p}})^{3}+|\sigma^{*}_{\mathrm{p}r}-r_{\mathrm{p}}|^{3}},$$

$$P_{\mathrm{e}}(r)=\frac{2r^{3}-3(\sigma^{*}_{\mathrm{p}r}+r_{\mathrm{p}})r^{2}-2r_{\mathrm{p}}^{3}+|\sigma^{*}_{\mathrm{p}r}-r_{\mathrm{p}}|^{3}}{-2r_{\mathrm{p}}^{3}+(\sigma^{*}_{\mathrm{p}r}+r_{\mathrm{p}})^{3}+|\sigma^{*}_{\mathrm{p}r}-r_{\mathrm{p}}|^{3}}, \tag{30}$$

where $\sigma^{*}_{\mathrm{p}i}=(2\sqrt{3})\sigma_{\mathrm{p}i}$ and r_{p} refers to the particle radial position. In order to evaluate the computational efficiency of the SPEED model, the modified SDDF model [14] was also used for Lagrangian computations. This model accounts for the effects of fluid turbulence anisotropy on discrete particle dispersion.

5. COMPUTATIONAL DETAILS

Shown in Figure 3 is the flow configuration together with the main geometric parameters. Experimental measurements indicate that the flow can be approximately assumed to be axisymmetric. Hence axisymmetric computations were carried out. To improve the mass flux prediction for axisymmetric two-phase flows, a drift correction algorithm developed by Chen and Pereira [14] was adopted to overcome the mass flux accumulation near the centreline.

The fluid Reynolds number was 5.6×10^{4} based on the maximum inlet fluid velocity and the smaller pipe diameter. The streamwise dimension for flow computation was taken to be 85 mm, starting from the pipe expansion. The computational domain was covered by a grid of 110×72 nodes in the streamwise and radial directions respectively. This grid was chosen as a result of grid independence tests. It was found that it gave a solution similar to that using 220×144 nodes. The initial conditions for the Eulerian equations were obtained by interpolating the measurements. The convective terms in these equations were discretized using a third-order QUICK algorithm. In the wall-adjacent region the conventional wall function method was used to modify the momentum equations and turbulent generations. The near-wall normal stresses were obtained by the usual solution of their corresponding equations under the assumption of zero diffusion to the wall. The numerical solution of the fluid phase was based upon a solution procedure developed by Patankar and Spalding [26]. Regarding the dispersed phase, the available detailed measurements at the inlet were used as input for initial Lagrangian conditions. Experimental measurements provided particle properties, such as mean and fluctuating velocities, at the inlet for radial positions 0, 1, 2, 3 and 4 mm from the centreline. Therefore the initial distribution of particle sizes and velocities was selected to

conform with the experimental measurements so that an adequate number of representative particles could be obtained. The particle–wall interaction was based on a simplified model [27]. To achieve a stochastically significant solution, 18 000 particle trajectories were tracked for the conventional SDDF model. However, 650 particle trajectories were tracked for the SPEED model. Therefore the number of particle trajectories used for the SPEED model is only 3.6% of that used for the SDDF model.

6. RESULTS AND DISCUSSION

Experimental measurements are available for several radial profiles of flow properties downstream of the inlet. Therefore these measured profiles were used to validate the present model predictions. Figure 4 shows the predicted and measured profiles of the liquid streamwise mean velocity at several downstream stations, ranging from $X = 1$ to 55 mm. Excellent agreement was achieved between the numerical predictions and the measurements, considering the slight

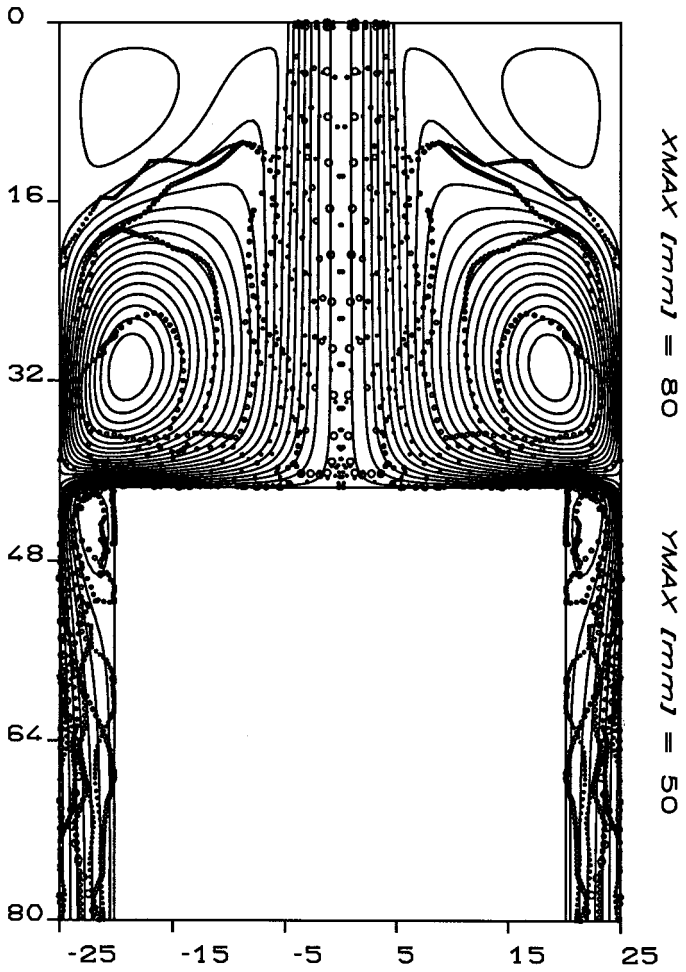

Figure 6. Liquid flow streamlines and particle trajectories

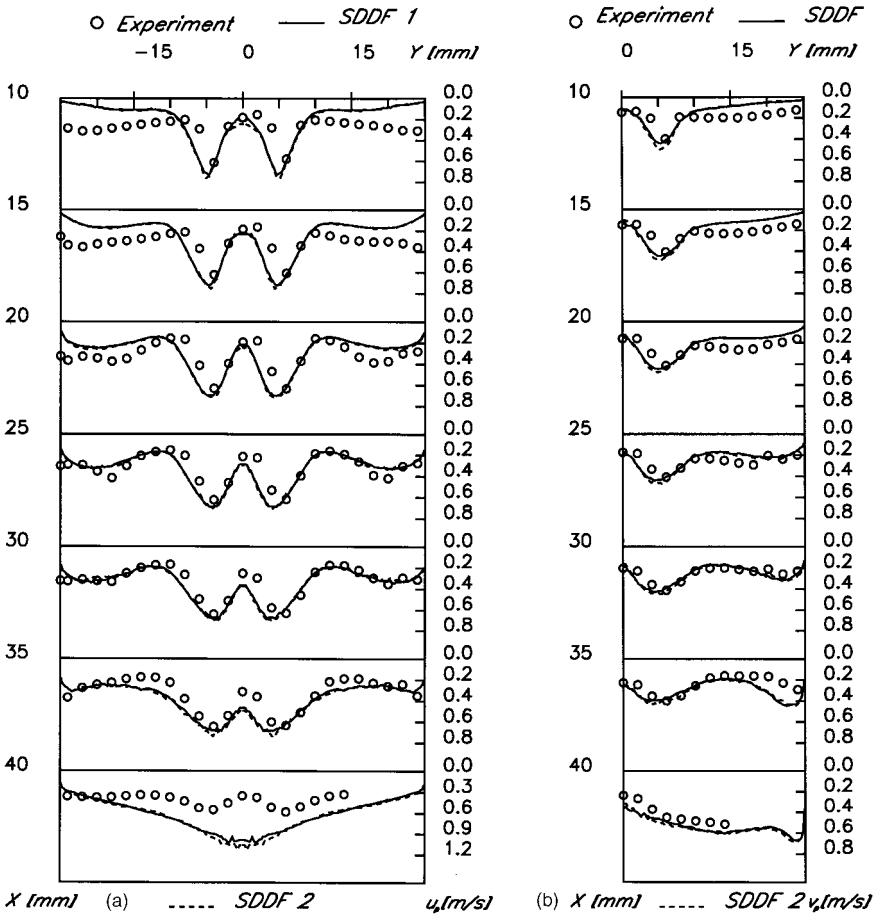

Figure 7. Effects of added mass term on (a) streamwise and (b) radial RMS velocities

asymmetry of the measurements. The streamwise and radial components of liquid fluctuating velocities are displayed in Figures 5(a) and 5(b) respectively. Overprediction of the normal stresses is observed for both streamwise and radial components. This may be attributed to the use of the standard second-moment closure model, which does not account for the effects of strong flow curvature caused by the centrebody. However, the anisotropy of turbulence was still captured with the present standard second-moment closure model.

To gain an intuitive impression of how particles interact with the fluid motion, Figure 6 shows the liquid flow streamlines together with some selected particle trajectories. Note that the symbol sizes in the figure are directly proportional to the real particle sizes. It can be seen that the largest particles are only slightly influenced by the liquid flow. However, the smallest particles are strongly influenced by the motion of the liquid flow. Such particle dispersion mechanisms have been explained by Crowe *et al.* [28] using a Stokes number defined as the ratio of the particle relaxation time to the flow characteristic time. The larger particles, with large Stokes numbers, are sluggish in following the motion of the fluid flow. They are moving directly downwards to impinge on the centrebody owing to their inertial effects. However, the smaller particles, with small Stokes numbers, are more responsive to the change in the fluid

flow. It can be seen that some of the particles can follow the vortical motion in the recirculating zone.

The effects of the added mass term on the predicted particle properties are shown in Figures 7(a) and 7(b) for the particle streamwise and radial RMS velocities respectively, where the full line (SDDF 1) represents the SDDF predictions accounting for the added mass term and the broken line (SDDF 2) denotes the SDDF predictions excluding the added mass term. It can be seen that the inclusion of the added mass term has improved the predicted particle RMS velocities. However, the improvement is not very pronounced. This is because of the predominant drag force in the equation of motion of a particle. It was found that the drag force preponderates over the added mass term owing to the very small particle relaxation time of (13). The effects of the added mass term on the particle number-mean diameter are shown in Figure 8. It is seen that the inclusion of the added mass term slightly improves the predicted diameter profiles. Note that the mean velocity profiles are not plotted here because no discernible descrepancy can be observed between the two predictions within plotting accuracy. In addition, it was found that the effect of the lift force on the predicted particle global properties is also relatively small, even though it had some influence on the motion of the individual particles.

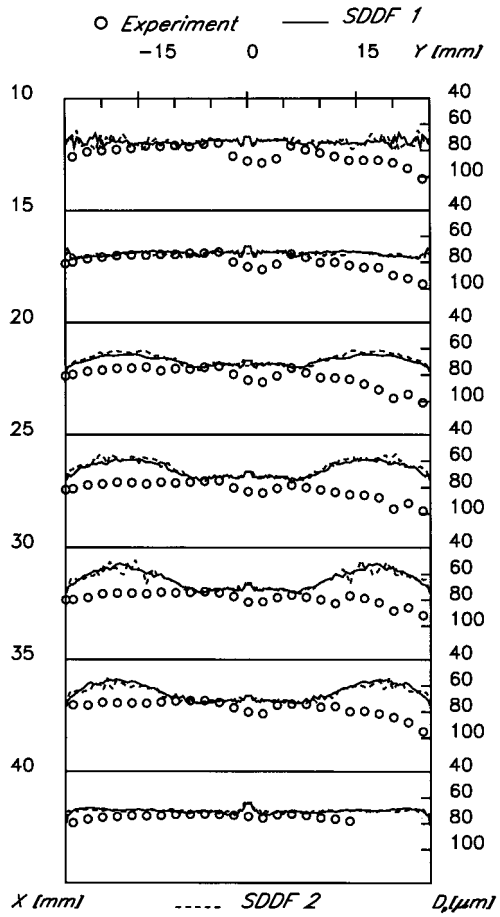

Figure 8. Effects of added mass term on particle number-mean diameter

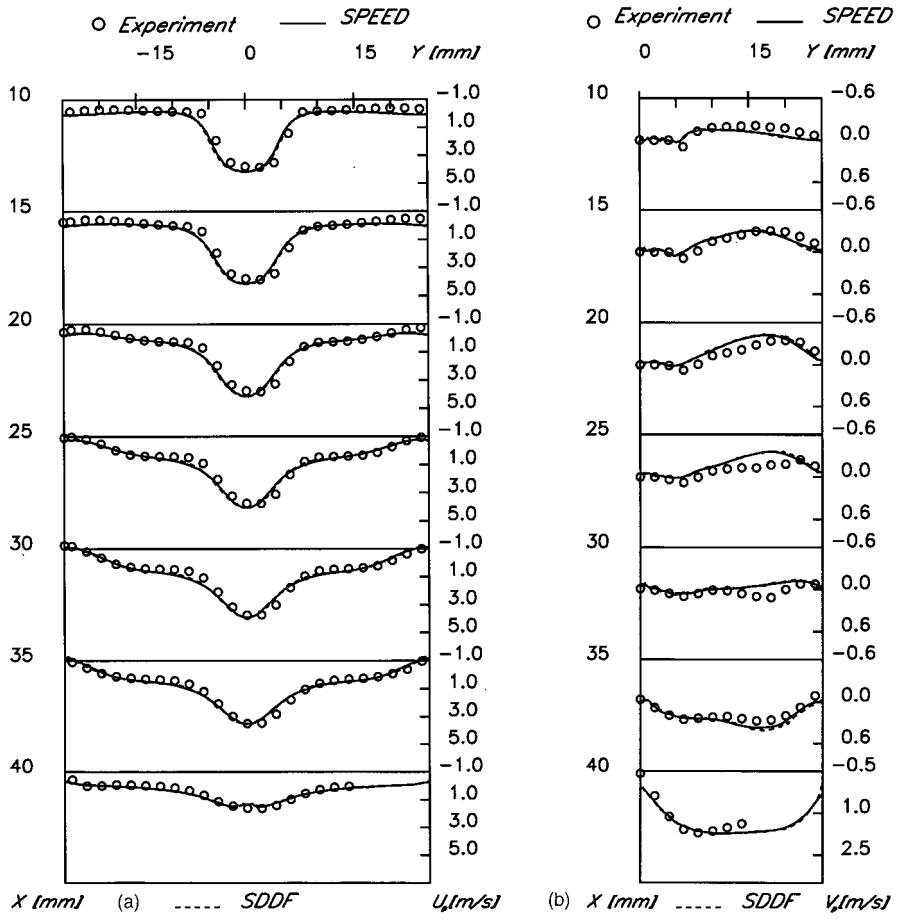

Figure 9. Two model predictions of (a) streamwise and (b) radial mean velocities

The evaluation of the SPEED model can now be obtained by comparing its predictions with the measurements [20]. It should be kept in mind that the SPEED model solely tracks 650 particle trajectories, i.e. much fewer than the 18 000 particle trajectories tracked by the SDDF model. As a reference, numerical results of the SDDF model are also presented together for direct comparison, and the following predictions have included the added mass term. It is known that the absolute computer CPU time depends on the computer itself. Therefore the relative time could be adequately used as a parameter to assess the efficiency of the SPEED and SDDF models. It was found that each Lagrangian tracking computation with the SPEED model required only about 8% of the CPU time needed by the SDDF model. Obviously, as far as the computational efficiency is concerned, the SPEED model is much more efficient than the SDDF model.

The accuracy and smoothness of the SPEED predictions are evaluated by presenting the radial profiles at different downstream stations and comparing them with available measurements. Figures 9(a) and 9(b) show the predicted and measured radial profiles of the particle streamwise and radial mean velocities respectively. Note that the full line represents the SPEED predictions and the broken line stands for the SDDF predictions. It is evident that even though the particle trajectory numbers differ greatly between the two trajectory models,

only a slight descrepancy exists between their predictions. The two predictions are in good agreement with the experimental measurements. This also corroborates the conclusion [14] that particle mean velocities are usually not sensitive to the number of particle trajectories.

The particle fluctuating velocities predicted with the SPEED and SDDF models are compared in Figures 10(a) and 10(b), together with the measurements, for the streamwise and radial components respectively. For the radial fluctuating velocity the two model predictions are slightly different from each other and are in satisfactory agreement with the experimental measurements, though slightly better agreement is obtained with the SPEED model. Of particular note is that the radial profiles of the SPEED predictions are smoother than those of the SDDF model, even though they are obtained using only 650 particle trajectories. This behaviour is attributed to the probabilistic procedure used in the SPEED model. Figure 10(a) indicates that the streamwise particle fluctuating velocity is overpredicted by the SPEED model compared with the SDDF model, regardless of the smoother profiles yielded by the SPEED model. This behaviour can be explained by the overpredicted fluid fluctuating velocities, shown in Figures 5(a) and 5(b), and by the expression of (17) which suggests that the particle trajectory variance is proportional to the fluid normal stresses. Therefore overpredicted fluid

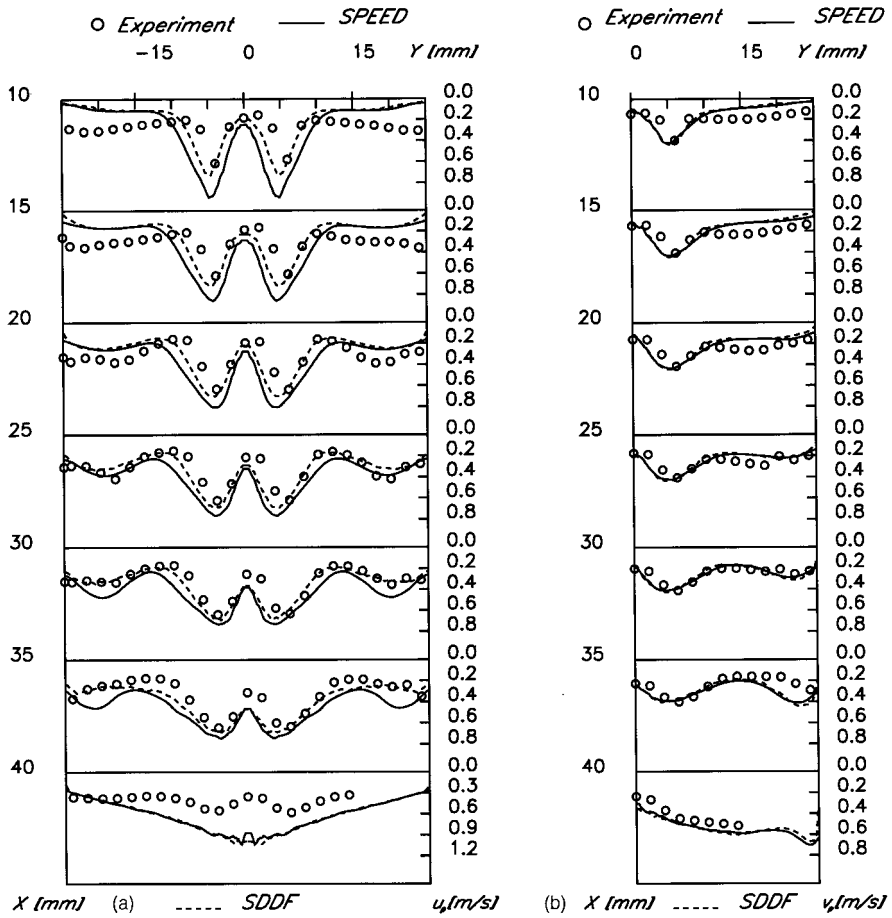

Figure 10. Two model predictions of (a) streamwise and (b) radial RMS velocities

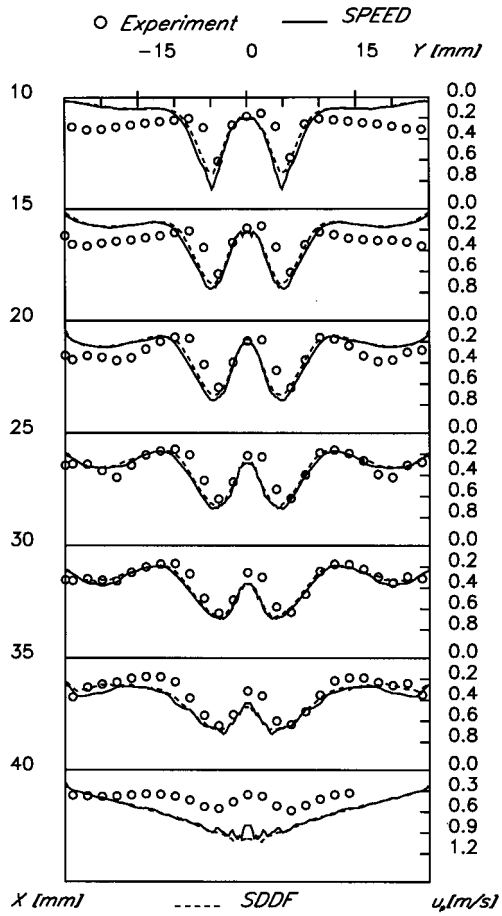

Figure 11. SPEED predictions of streamwise RMS velocity using reduced variance

normal stresses will lead to overpredicted particle trajectory variances. As a result, the computed particle dispersion in the SPEED model is overpredicted. Such reasoning can be proven by using a reduced particle trajectory variance. Figure 11 shows the radial profiles of the particle streamwise fluctuating velocity predicted using 85% of the computed radial trajectory variance. It is clear that the overpredicted particle streamwise fluctuating velocity in Figure 10(a) is improved as a result.

Figure 12 shows the evolving radial profiles of the particle number-mean diameter. It is demonstrated that much smoother profiles are obtained with the SPEED model. Of interest is that the experimental measurements exhibit some asymmetry and that the numerical predictions show a larger deviation from the measurements between $X = 20$ and 35 mm than in the other region. This is mainly attributed to the unfavourable influence of flow recirculation there; see Figure 6. Theoretically, only small particles having small Stokes numbers are responsive to the change in liquid flow, as explained by Crowe *et al.* [28]. For the flow studied, the larger particles having larger Stokes numbers are not easily influenced by the gas flow, but move directly downwards owing to larger inertia. As a result, a small particle mean diameter is present in the recirculating zone. Therefore the numerical predictions are physically reasonable.

There must be some experimental errors in the diameter measurements. Finally, the profiles of the predicted particle mass flux are compared in Figure 13. The two model predictions are generally agreeable. Once again the measurements are axisymmetric, especially in the region between $X = 20$ and 35 mm.

7. CONCLUDING REMARKS

An efficient Lagrangian trajectory model (SPEED) was employed to predict particle dispersion in a turbulent liquid flow. This model overcomes the drawbacks of conventional stochastic discrete-delta-function models but retains their advantages. The SPEED model is characterized by its high computational efficiency, accurate numerical predictions and simple theoretical background, which makes it easy to incorporate into existing Lagrangian stochastic models. To achieve a stochastically significant solution, it was found that the SPEED model required tracking a substantially smaller number of particle trajectories than the stochastic discrete-delta-function model. Concerning computer CPU time, it was found that each Lagrangian

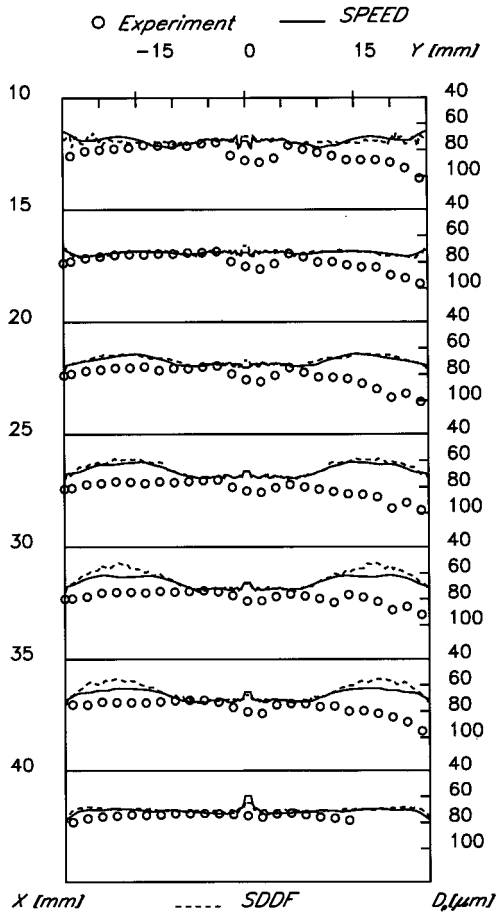

Figure 12. Two model predictions of particle number-mean diameter

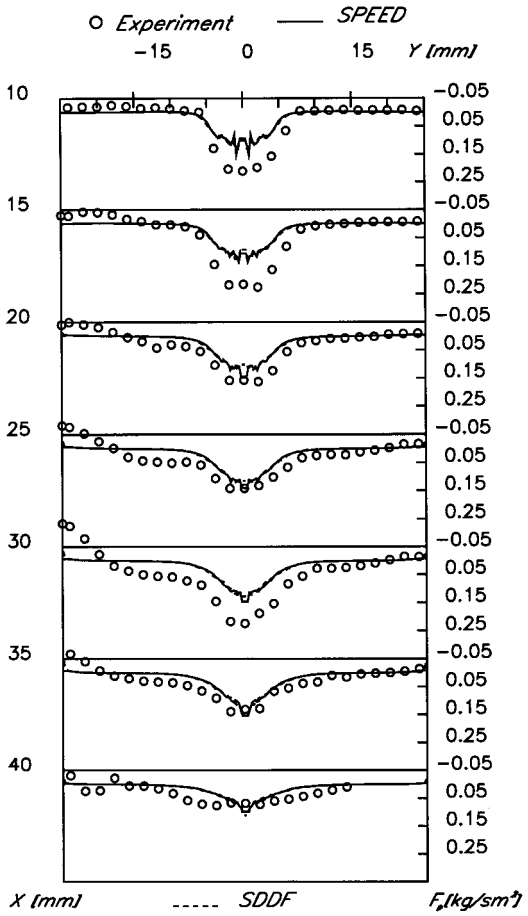

Figure 13. Two model predictions of particle mass flux

tracking computation using the SPEED model required only about 8% of the computer CPU time needed by the SDDF model for the present flow, thus substantially enhancing the computational efficiency of Lagrangian trajectory calculations. In addition, it was found that the numerical results of the SPEED and SDDF models generally agreed, even though there was a large difference in the numbers of particle trajectories tracked. Furthermore, it was found that the slightly overpredicted particle streamwise fluctuating velocity by the SPEED model can be attributed to the overpredicted liquid phase fluctuating velocities. This difficulty, however, may be overcome by using improved versions of turbulent Reynolds stress models.

ACKNOWLEDGEMENTS

Dr. Chen would like to gratefully acknowledge the research grant received from the Portuguese foundation JNICT in the framework of PRAXIS XXI, and the data from C. Freek.

APPENDIX A. NOMENCLATURE

C_β model constant (= 0.85)
D_p particle diameter
k turbulent kinetic energy
P pressure
t time
U axial mean velocity
V radial mean velocity
x axial co-ordinate
y, r radial co-ordinate

Greek letters

ε dissipation rate of k
μ laminar dynamic viscosity
ρ density
σ_p model constant (= 1.5)

Subscripts

i, j, k Cartesian components
p particle phase

Superscripts

l lower boundary
u upper boundary

REFERENCES

1. J.-S. Shuen, A.S.P. Solomon, Q.-F. Zhang and G.M. Faeth, 'Structure of particle-laden jets: measurements and predictions', *AIAA J.*, **23**, 396–404 (1985).
2. G. Hetsroni, 'Particles–turbulence interaction', *Int. J. Multiphase Flow*, **15**, 735–746 (1989).
3. A. Berlemont, P. Desjonqueres and G. Gouesbet, 'Particle Lagrangian simulation in turbulent flows', *Int. J. Mutliphase Flow*, **16**, 19–34 (1990).
4. C.P. Chen, H.M. Shang and Y. Jiang, 'An efficient pressure–velocity procedure for gas–droplet two-phase flow calculations', *Int. j. numer. meth. fluids*, **15**, 233–245 (1992).
5. Y. Tsuji, 'Discrete particle simulation of gas–solid flows', *KONA Power Part.*, **11**, 57–68 (1993).
6. K.-C. Chang and W.-J. Wu, 'Sensitivity study on Monte Carlo solution procedure of two-phase turbulent flows', *Numer. Heat Transfer*, **25**, 223–244 (1994).
7. Y. Sato, K. Hishida and M. Maeda, 'Effect of dispersed phase on modification of turbulent flow in a wall jet', *J. Fluids Engng.*, **118**, 307–315 (1996).
8. X.-Q. Chen, C. Freek and J.C.F. Pereira, 'Experimental and numerical study of a water spray in the wake of an axisymmetric bluff body', *Exp. Thermal Fluid Sci.*, **13**, 129–141 (1996).
9. C.T. Crowe, T.R. Troutt and J.N. Chung, 'Numerical models for two-phase turbulent flows', *Ann. Rev. Fluid Mech.*, **28**, 11–43 (1996).
10. I.E. Barton, 'Computation of dilute particulate laminar flow over a backward-facing step', *Int. j. numer. meth. fluids*, **22**, 211–221 (1996).

11. P. Creismeas, 'A Eulerian/Lagrangian model to calculate the evolution of a water droplet spray', *Int. j. numer. meth. fluids*, **20**, 135–155 (1995).
12. A.A. Mostafa, H.C. Mongia, V.G. McDonell and G.S. Samuelsen, 'Evolution of particle-laden jet flows: a theoretical and experimental study', *AIAA J.*, **27**, 167–183 (1989).
13. A. Adeniji-Fashola and C.P. Chen, 'Modeling of confined turbulent fluid–particle flows using Eulerian and Lagrangian schemes', *Int. J. Heat Mass Transfer*, **33**, 691–701 (1990).
14. X.-Q. Chen and J.C.F. Pereira, 'Computation of turbulent evaporating sprays with well-specified measurements; a sensitivity study on droplet properties', *Int. J. Heat Mass Transfer*, **39**, 441–454 (1996).
15. X.-Q. Chen and J.C.F. Pereira, 'Efficient computation of particle dispersion in turbulent flows with a stochastic–probabilistic model', *Int. J. Heat Mass Transfer*, **40**, 1727–1741 (1997).
16. A.D. Gosman and E. Ioannides, 'Aspects of computer simulation of liquid-fuelled combustors', *AIAA Paper 81-0323*, 1981.
17. A.S.P. Solomon, J.-S. Shuen, Q.-F. Zhang and G.M. Faeth, 'Structure of nonevaporating sprays, Part I: Initial conditions and mean properties', *AIAA J.*, **23**, 1548–1555 (1985).
18. X.-Q. Chen and J.C.F. Pereira, 'Numerical prediction of evaporating and nonevaporating sprays under nonreactive conditions', *Atomiz. Sprays*, **2**, 427–443 (1992).
19. N.G. Muoio, C.T. Crowe, U. Fritsching and D. Bergmann, 'Effect of thermal coupling on numerical simulations of the spray forming process', *ASME FED*, **236**, 233–237 (1996).
20. C. Freek, 'Experimental investigation of single and two-phase flows in the wake of an axisymmetric bluffbody', *M.S. Thesis*, Instituto Superiro Técnico, Lisbon, 1995.
21. M.A. Rizk and S.E. Elghobashi, 'A two-equation turbulence model for dispersed dilute confined two-phase flow', *Int. J. Multiphase Flow*, **15**, 119–133 (1989).
22. F. Durst, D. Milojevic and B. Schonung, 'Eulerian and Lagrangian predictions of particulate two-phase flows: a numerical study', *Appl. Math. Model.*, **8**, 101–115 (1984).
23. R.J. Litchford and S.-M. Jeng, 'Efficient statistical transport model for turbulent particle dispersion in sprays', *AIAA J.*, **29**, 1443–1451 (1991).
24. R.J. Litchford and S.-M. Jeng, 'Probability density function shape sensitivity in the statistical modeling of turbulent particle dispersion', *AIAA J.*, **30**, 2546–2549 (1992).
25. X.-Q. Chen and J.C.F. Pereira, 'Numerical study of a nonevaporating polydispersed turbulent hollow-cone spray', *ASME FED*, **236**, 41–50 (1996).
26. S.V. Patankar and D.B. Spalding, 'A calculation procedure for heat, mass and momentum transfer in three-dimensional parabolic flows', *Int. J. Heat Mass Transfer*, **15**, 1787–1806 (1972).
27. J.L.T. Azevedo and J.C.F. Pereira, 'Prediction of gas–particle turbulent free or confined jet flows', *Part. Part. Syst. Charact.*, **7**, 171–180 (1990).
28. C.T. Crowe, J.N. Chung and T.R. Troutt, 'Particle mixing in free shear flows', *Prog. Energy Combust. Sci.*, **14**, 171–194 (1988).

